Can we improve the cross sections calculation for deuteron induced reactions ?
Or the deuteron induced reactions within the CDCC formalism: from differential cross sections to excitation functions?

CHAU HUU-TAI Pierre

CEA/DAM/DIF

$P(ND)^2$-2 - October 2014

Introduction.

Deuteron induced reactions are useful tools

1. to investigate nuclear structure via elastic, inelastic or transfer reactions;
2. to produce isotopes relevant for medical or technological applications.

It is important to build models which can accurately predict the d+A cross sections. Some improvements remain to be achieved. We reproduce a comparison between some TENDL-2011 calculations and Exfor data from the Janis book of d induced cross sections by N. Soppera *et al* [1].

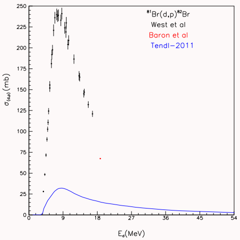

Figure: ^{81}Br(d,p).

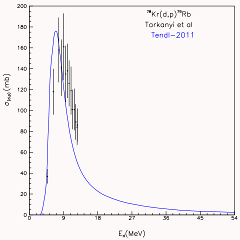

Figure: ^{78}Kr(d,n).

These cross sections are difficult to compute due to the deuteron features: its a weakly bound composite system. A formalism now known as the CDCC approach has been proposed to include these properties.

CDCC formalism with elastic and elastic breakup channels: a brief overview (1).

A detailled description can be found e.g. in [2, 3].
In CDCC, it is assumed that the $(A+2)$-body system can be described by the following three-body phenomenological hamiltonian

$$\hat{H}_{eff} = \hat{T}_{\vec{R}} + U_{pA}(\vec{r}_p, E/2) + U_{nA}(\vec{r}_n, E/2) + \underbrace{\hat{T}_{\vec{\rho}} + V_{pn}(\vec{\rho})}_{\hat{H}_{pn}} + V_p^{(Coul)}(R)$$

where

$$\vec{R} = (\vec{r}_p + \vec{r}_n)/2 \text{ and } \vec{\rho} = \vec{r}_n - \vec{r}_p \,.$$

are respectively center-of-mass and relative motion coordinates while $\hat{T}_{\vec{R}}$ and $\hat{T}_{\vec{\rho}}$ are the associated kinetic-energy operators. $\hat{H}_{pn}$ denotes the proton-neutron interaction and the U_{iA} the nucleon-target interactions.

$$\mathbf{J} = L + \mathbf{I} \,;\, \mathbf{I} = l + \mathbf{S} \text{ and } \mathbf{S} = \mathbf{s}_p + \mathbf{s}_n$$

wil denote the total angular momentum, and L and $\mathbf{I}$ are respectively associed with $\vec{R}$ and $\vec{\rho}$. $\mathbf{S}$ and l are respectively the proton-neutron spin and orbital angular momentum.

CDCC formalism with elastic and elastic breakup channels: a brief overview (2).

The three-body wave function with the total angular momentum J and its projection M is eigenstate of this Hamiltonian (1) and can be expanded as follows

$$\Psi_{JM} = \sum_{L=|J-1|}^{J+1} \left[\Phi_0(\vec{\rho}) \otimes \chi_0(L, J\,;\, \vec{R})\right]_{JM}$$
$$+ \sum_{l=0}^{\infty} \sum_{I=|l-S|}^{l+S} \sum_{L=|J-I|}^{J+I} \underbrace{\int_0^{\infty} \left[\Phi(^{2S+1}l_I\,;\, k, \vec{\rho}) \otimes \chi(^{2S+1}l_I, L, J\,;\, P_k, \vec{R})\right]_{JM} dk}_{BU}$$

where Φ_0 is the deuteron ground state and the $\Phi(^{2S+1}l_I\,;\, k, \vec{\rho})$ are continuum states of a p-n broken pair. These functions respectively satisfy the equations:

$$\hat{H}_{pn}\Phi_0(\vec{\rho}) = \varepsilon_0\Phi_0(\vec{\rho}) \text{ and } \hat{H}_{pn}\Phi(^{2S+1}l_I\,;\, k, \vec{\rho}) = \varepsilon_k\Phi(^{2S+1}l_I\,;\, k, \vec{\rho})\,,\ \varepsilon_k = \frac{\hbar^2 k^2}{2\mu_\rho}\,,$$

where μ_ρ is the p-n reduced mass, k denotes the relative momentum between n and p and ε_0 the ground state energy. Then the deuteron motion with momentum P_0 is described by χ_0 and the motion of a broken pair with momentum P_k by $\chi(^{2S+1}l_I, L, J\,;\, P_k, \vec{R})$ which means that the first term of (2) denotes the elastic channel whereas the second one, BU, represents the breakup channels.

CDCC formalism with elastic and elastic breakup channels: a brief overview (3).

In the CDCC formalism, the following hypothesis are made:

- The continuum is discretized into bins $[k_i, k_{i+1}]$ and it is assumed that on each sub-interval

$$\chi(^{2S+1}l_l, L, J\,;\, P_k, \vec{R}) \sim \chi(^{2S+1}l_l, L, J\,;\, \tilde{P}_i, \vec{R})\,, \forall k \in [k_i, k_{i+1}]$$

$$\begin{aligned} BU &= \int_0^{\infty} \left[\Phi(^{2S+1}l_l\,;\, k, \vec{\rho}) \otimes \chi(^{2S+1}l_l, L, J\,;\, P_k, \vec{R})\right]_{JM} dk \\ &\sim \sum_{i=1}^{\infty} \int_{k_i}^{k_{i+1}} \left[\Phi(^{2S+1}l_l\,;\, k, \vec{\rho}) \otimes \chi(^{2S+1}l_l, L, J\,;\, \tilde{P}_i, \vec{R})\right]_{JM} dk \\ BU &= \sum_{i=1}^{\infty} \left[\tilde{\Phi}_i(^{2S+1}l_l\,;\, \vec{\rho}) \otimes \tilde{\chi}_i(^{2S+1}l_l, L, J\,;\, \vec{R})\right]_{JM} \end{aligned}$$

with $\tilde{\Phi}_i(^{2S+1}l_l\,;\, \vec{\rho}) = \dfrac{1}{\sqrt{k_{i+1} - k_i}} \displaystyle\int_{k_i}^{k_{i+1}} \Phi_i(^{2S+1}l_l\,;\, k, \vec{\rho})\, dk$

and $\tilde{\chi}_i(^{2S+1}l_l, L, J\,;\, \vec{R}) = \sqrt{k_{i+1} - k_i}\, \chi(^{2S+1}l_l, L, J\,;\, \tilde{P}_i, \vec{R})\,,$

$$E = \hbar^2 \tilde{P}_i^2 / 2\mu_R + \varepsilon_{\tilde{k}_i} \text{ with } \tilde{k}_i = (k_{i+1} - k_i)^2/12 + (k_i + k_{i+1})^2/4\,.$$

CDCC formalism with elastic and elastic breakup channels: a brief overview (4).

In the CDCC formalism, it is also assumed that

- The model space can be truncated by taking into account only waves with $l \leq l_{max}$ and $k \leq k_{max}$ (i_{max}) thus the three-body wave function becomes :

$$\tilde{\Psi}_{JM} = \sum_{L=|J-1|}^{J+1} \left[\Phi_0(\vec{\rho}) \otimes \chi_0(L, J;\, \vec{R}) \right]_{JM} + \sum_{I,L,l} \sum_{i=0}^{i_{max}} \left[\tilde{\Phi}_i({}^{2S+1}l_I\,; \vec{\rho}) \otimes \tilde{\chi}_i({}^{2S+1}l_I, L, J;\, \vec{R}) \right]_{JM} .$$

By left-multiplying by $\left[\tilde{\Phi}_i({}^{2S+1}l_I\,; \vec{\rho}) \otimes Y_L(\hat{R}) \right]_{JM}$ and integrating over $\vec{\rho}$ and the angular variables $\hat{R}$, one gets the following set of coupled differential equations satisfied by the radial parts $u_c^J(R)$ ($c = (i, l, S, I, L, J)$) of the wave functions :

$$\left(-\frac{\hbar^2}{2\mu_R}\frac{d^2}{dR^2} + \frac{\hbar^2 L(L+1)}{2\mu_R R^2} + V_p^{(Coul)} - E_i \right) u_c^J(R) = -\sum_{c'} F_{cc'}^J(R) u_{c'}^J(R) ,$$

where the form factors are defined by

$$F_{cc'}^J(R) = \langle \left[\tilde{\Phi}_i \otimes Y_L(\hat{R}) \right]_{JM} | U_{pA} + U_{nA} | \left[\tilde{\Phi}_{i'} \otimes Y_{L'}(\hat{R}) \right]_{JM} \rangle_{\hat{R},\hat{\rho},\rho} .$$

In equation (4), the brackets $\langle\,\rangle_{\hat{R},\hat{\rho},\rho}$ denote the integration over $\vec{\rho}$ and the solid angle $\hat{R}$.

CDCC formalism with elastic and elastic breakup channels: a brief overview (5).

These form factors are computed by expanding the potentials into multipoles:

$$U_{iA}(|\vec{R} \pm \vec{\rho}/2|) \quad = \quad \sum_{\lambda} U_{iA}^{(\lambda)} P_{\lambda}(\cos(\theta))$$

where i denotes proton or neutron and θ the angle between $\vec{R}$ and $\vec{\rho}$.
The solutions of the CDCC equations (11) must satisfy the following boundary condition

$$u_c^J(R) \to \delta_{c_0 c}\, U^{(-)}(\tilde{P}_i R) - \sqrt{\tilde{P}_i/\tilde{P}_0}\, \hat{S}_{c_0 c}^{(J)}\, U^{(+)}(\tilde{P}_i R)\,,$$

where $\hat{S}_{c_0 c}^{(J)}$ are the CDCC S-matrix elements, c_0 denotes the elastic channel and $U^{(+)}$ and $U^{(-)}$ are respectively the outgoing and incoming Coulomb wave functions.
Note that in (11) the Coulomb interaction is acting on the center-of-mass coordinates as usually assumed in the literature.

Ground state and binding energy.

We investigate the effect of the shape of the ground state wave functions and of the binding energy on the cross section calculations. These calculations are performed assuming that:

- The target is the ^{58}Ni.
- The nucleon-target optical potentials are those proposed by A. Koning and J.-P. Delaroche.
- The deuteron ground state is calculated with the V_{pn} interaction with a Gaussian shape for 3 sets of parameters: three different wave functions have been obtained with
  - $\varepsilon_{\mathrm{g.s.}} = -0.68$ MeV,
  - $\varepsilon_{\mathrm{g.s.}} = -2.22$ MeV
  - and $\varepsilon_{\mathrm{g.s.}} = -4.32$ MeV.
- The incident energy ranges between 5 MeV and 80 MeV.

Calculations with different g.s. wave functions.

The radial part of the g.s. w.f.

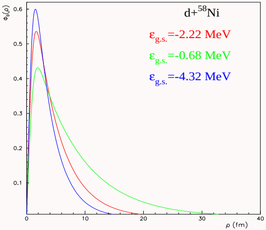

Form factor obtained by folding.

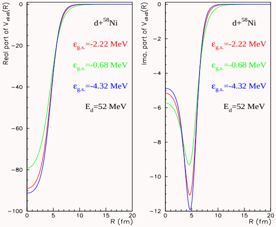

Reaction cross sections.

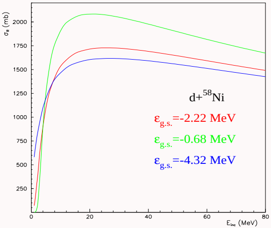

Differential cross section.

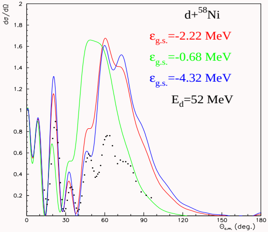

Differential cross section.

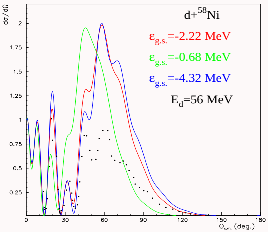

Differential cross section.

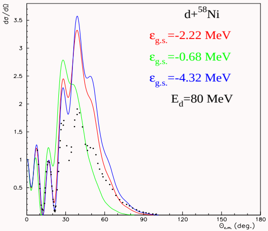

Effect of the projectile wave function.

From these figures, we can draw the following conclusions:

1. The depth and the width of folding potentials are modified.
2. The threshold and the amplitude of the reaction cross sections depend strongly on this w.f.
3. The oscillary patterns of the differential cross sections also depend on the projectile w.f.

An accurate measurement of the cross sections can thus provide a precise insight about the projectile features.

Continuum effect.

We want to check that the CDCC approach converges while increasing the number of states (i.e. the number of bins) used to discretize the continuum. We also wish to compare the calculated cross section with the experimental one. The following calculations are performed assuming that:

- The target is the ^{58}Ni.
- The nucleon-target optical potentials are those proposed by A. Koning and J.-P. Delaroche.
- The *s* and *d* waves of the deuteron g.s. and p-n continuum states are obtained by using the Reid93 potential.
- The deuteron is incident at 80 MeV on the target.
- The number of bins increases from 0 to 12.
- k_{max}=1.5 fm^{-1}.

Convergence of the CDCC calculations with the bin number.

Differential cross section.

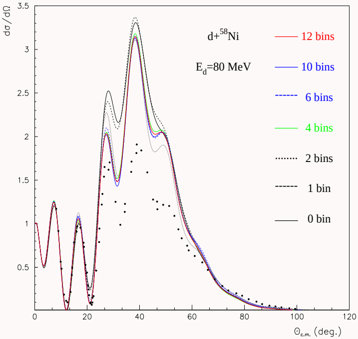

Differential cross section (log scale).

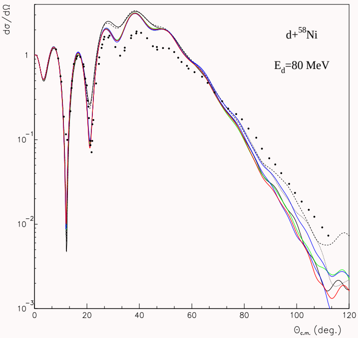

Continuum effect.

We can conclude that:

1. The calculations converge while increasing the bin number.
2. For this incident energy, the elastic cross section calculation has converged by using 4 bins to describe the continuum .
3. A better agreement with the experimental data is obtained by including the continuum states.

As expected for weakly bound projectile, the coupling to continuum states plays a crucial role onto the elastic cross sections and it clearly improves the agreement with the experimental data even though there are still some discrepancies between the calculated cross section and the experimental one meaning that other channels (inelastic, transfer ?) should be included.

Concluding remarks

These calculations show that:

1. The calculated cross sections depend on the shape of the projectile wave function.
2. The CDCC cross sections converge while increasing the bin number.
3. The coupling between the elastic channel and the breakup ones has to be included to improve the agreement between calculations and experimental data.
4. It seems important to include all the open channels to describe the continuum.
5. It seems also that it is necessary to go beyond CDCC calculations and to include other reaction channels :
   - the channels describing the projectile excitations (XCDCC)?
   - the inelastic channels to take into account the target excitations (CDCC*)?
   - the transfer channels?

Target excitations: CDCC* - The 3-body wave function.

We propose to extend the CDCC approach for d induced reaction to include with the target excitations within the coupling scheme. The new wave function reads as:

$$|\Psi_{J_T M_T}(\vec{R},\vec{\rho})\rangle = \sum_{i\,l\,S\,I_p\,L\,J\,I_t} |(i\,l\,S)\,I_p\,L\,JI_t\,;J_T\,M_T\rangle$$

where $\vec{R}$ denotes the deuteron center of mass coordinates and $\vec{\rho}$ the proton-neutron relative coordinates. The channels of the system for a given J_T are characterized by the following quantum numbers:

- The bin number i to discretize the continuum;
- The deuteron spin $S = 1$;
- The relative orbital angular momentum l associated to $\vec{\rho}$;
- The angular momentum J;
- The orbital angular momentum L associated to $\vec{R}$;
- The spin of the target I_t.

with $\vec{S} + \vec{l} = \vec{I_p}$, $\vec{L} + \vec{I_p} = \vec{J}$ and $\vec{I_t} + \vec{J} = \vec{J_T}$.

Target excitations: CDCC* - The new Schrödinger equation.

The previous wave function satisfies the following Schrödinger equation:

$$\hat{H}|\Psi_{J_T M_T}(\vec{R},\vec{\rho})\rangle = E|\Psi_{J_T M_T}(\vec{R},\vec{\rho})\rangle$$

where

$$\hat{H} = \hat{T}_R + V_{pA}(\vec{r}_p,\xi_t) + V_{nA}(\vec{r}_n,\,\xi_t) + V_{Coul} + \hat{H}_{pn} + \hat{H}_A$$

with

$$\hat{H}_{pn}\,\varphi_{il}(\vec{\rho}) = \varepsilon_i\,\varphi_{il}(\vec{\rho}),\ \hat{H}_A\,\psi_{I_t}(\xi_t) = \hat{\varepsilon}_{I_t}\,\psi_{I_t}(\xi_t)$$

and

$$V(\vec{r}_i,\,\xi_t) = V(r_i,\theta_i,\phi_i,\,\xi_t) = \sum_\lambda v^{(\lambda)}(r_i)P_\lambda(\cos(\theta_i'))\,.$$

Due to the deformation, for each nucleon, the optical potential depends on $\vec{r}_i$ ($i = n$ or p).

Rotating target - The starting point: T. Tamura's work [4].

The optical potential between the rotating target and a nucleon was derived by T. Tamura and is given by

$$V_{iA}(\vec{r}_i\,\xi_t) \;=\; \sum_{\lambda}\sum_{\mu=-\lambda}^{\lambda} v^{(\lambda)}(r_i) D^{\lambda}_{\mu 0}(\Theta_j) Y^{\lambda}_{\mu}(\hat{r}_i)\,.$$

where Θ_j denote the Euler angles.

The solid spherical harmonics addition theorem for $\vec{r}_i = x_i\vec{R} + y_i\vec{\rho}$

$$r_i^{\lambda} Y^{\lambda}_{\mu}(\hat{r}_i) = \sum_{0\le p\le\lambda} \frac{\sqrt{4\pi(2\lambda+1)!}\,x_i^p R^p y_i^p \rho^{\lambda-p}}{\sqrt{(2p+1)!(2(\lambda-p)+1)!}} \left[Y^p(\hat{R})\otimes Y^{\lambda-p}(\hat{\rho})\right]^{\lambda}_{\mu}\,.$$

Thus, the equation (6) can be transformed into:

$$V_{iA}(\vec{r}_i\,\xi_t) \;=\; \sum_{\lambda}\sum_{\mu=-\lambda}^{\lambda} D^{\lambda}_{\mu 0}(\Theta_j) v^{(\lambda)}(r_i) \sum_{p=0}^{\lambda} C_{\lambda p} \frac{x_i^p R^p y_i^{\lambda-p}\rho^{\lambda-p}}{r_i^{\lambda}} \left[Y^p(\hat{R})\otimes Y^{\lambda-p}(\hat{\rho})\right]^{\lambda}_{\mu}\,,$$

where $C_{\lambda p} = \sqrt{\dfrac{4\pi(2\lambda+1)!}{(2p+1)!(2(\lambda-p)+1)!}}$, while $\vec{r}_i = x_i\vec{R} + y_i\vec{\rho}$ ie $x_i = 1$ and $y_i = \pm 1/2$.

Rotating target - The multipole expansion.

To simplify (7), a multipole expansion of its radial terms can be performed

$$\frac{v^{(\lambda)}(r_i) x_i^p R^p y_i^{\lambda-p} \rho^{\lambda-p}}{r_i^\lambda} = \sum_\sigma (-1)^\sigma \frac{4\pi}{\hat{\sigma}} v_p^{(\lambda)\sigma}(r,\rho) \left[Y^\sigma(\hat{R}) \otimes Y^\sigma(\hat{\rho}) \right]_0^0 .$$

Then equation (7) reads as

$$\begin{aligned} V_{iA}(\vec{r}_i\, \xi_t) &= \sum_\lambda \sum_{\mu=-\lambda}^{\lambda} \sum_{p=0}^{\lambda} \sum_\sigma C_{\lambda p} (-1)^\sigma \frac{4\pi}{\hat{\sigma}} D_{\mu 0}^\lambda(\Theta_j) v_p^{(\lambda)\sigma}(r,\rho) \\ & \left[Y^\sigma(\hat{R}) \otimes Y^\sigma(\hat{\rho}) \right]_0^0 \left[Y^p(\hat{R}) \otimes Y^{\lambda-p}(\hat{\rho}) \right]_\mu^\lambda . \end{aligned}$$

It can also be shown that:

$$\left[Y^\sigma(\hat{R}) \otimes Y^\sigma(\hat{\rho}) \right]_0^0 \left[Y^p(\hat{R}) \otimes Y^{\lambda-p}(\hat{\rho}) \right]_\mu^\lambda = (-1)^\lambda \sum_{l'' L''} \frac{\hat{\sigma} \widehat{l''} \widehat{L''} \hat{p} \widehat{(\lambda-p)}}{4\pi}$$

$$\begin{pmatrix} \sigma & p & L'' \\ 0 & 0 & 0 \end{pmatrix} \begin{pmatrix} \sigma & (\lambda-p) & l'' \\ 0 & 0 & 0 \end{pmatrix} \begin{Bmatrix} \lambda & L'' & l'' \\ \sigma & p & (\lambda-p) \end{Bmatrix} \left[Y^{L''}(\hat{R}) \otimes Y^{l''}(\hat{\rho}) \right]_\mu^\lambda ,$$

where $|\lambda - p - \sigma| \leq L'' \leq \lambda - p + \sigma$ and $|p - \sigma| \leq L'' \leq p + \sigma$.

Rotating target - Multipole expansion.

The nucleon-nucleus optical potentials look like

$$V_{iA}(\vec{r}_i\,\xi_t) = \sum_{\lambda\,\mu\,p\,\sigma\,l''\,L''} (-1)^{\lambda+\sigma} D^{\lambda}_{\mu 0}(\Theta_j) C_{\lambda p} \widehat{l''}\,\widehat{L''}\,\hat{p}\,\widehat{(\lambda-p)} \begin{pmatrix} \sigma & p & L'' \\ 0 & 0 & 0 \end{pmatrix}$$

$$\begin{pmatrix} \sigma & (\lambda-p) & l'' \\ 0 & 0 & 0 \end{pmatrix} \qquad \begin{Bmatrix} \lambda & L'' & l'' \\ \sigma & p & (\lambda-p) \end{Bmatrix} v_p^{(\lambda)\sigma}(R,\rho) \left[Y^{L''}(\hat{R}) \otimes Y^{l''}(\hat{\rho}) \right]^{\lambda}_{\mu}.$$

This equation (9) is convenient since there is a separation between the radial variables, the angular variables and target ones. Thus the computation of the coupling between different channels can be quite straightfowardly performed by using the Wigner-Eckart theorem

Rotating target - Form factors.

If c and c' denote the channels $|(i\,l\,S)\,I_p\,L\,J I_t\,;J_T\,M_T\rangle$ and $|(i'\,l'\,S')\,I'_p\,L'\,J'\,I'_t\,;J_T\,M_T\rangle$ respectively then the form factor $V_{c\,c'} = \langle c|V(\vec{r}_i)|c'\rangle$ is given by:

$$\begin{aligned} V_{c\,c'}(R) &= \frac{1}{4\pi}\sum_{\lambda\,p\,\sigma\,l''\,L''} \delta_{s\,s'}(-1)^{L'+l'}(-1)^{\sigma+I'_t}\hat{l}\hat{I}_p\hat{L}\hat{J}\hat{I}_t\hat{l'}\hat{I'_p}\hat{L'}\hat{J'}\hat{I'_t} \\ & \widehat{l''}^2\widehat{L''}^2\widehat{(\lambda-p)}\hat{p}\,(-1)^{J_T+M_T}\begin{Bmatrix} L & I_p & J \\ L'' & l'' & \lambda \\ L' & I'_p & J' \end{Bmatrix}\begin{pmatrix} \sigma & p & L'' \\ 0 & 0 & 0 \end{pmatrix} \\ & \begin{pmatrix} \sigma & (\lambda-p) & l'' \\ 0 & 0 & 0 \end{pmatrix}\begin{pmatrix} L & L'' & L' \\ 0 & 0 & 0 \end{pmatrix}\begin{pmatrix} l & l'' & l' \\ 0 & 0 & 0 \end{pmatrix}\begin{Bmatrix} \lambda & L'' & l'' \\ \sigma & p & (\lambda-p) \end{Bmatrix} \\ & \begin{Bmatrix} I'_p & l'' & I_p \\ l & s & l' \end{Bmatrix}\begin{Bmatrix} I_t & I'_t & \lambda \\ J' & J & J_T \end{Bmatrix}\int u_{i'l'}(\rho)u_{il}(\rho)v_p^{(\lambda)\sigma}(R,\rho)d\rho\,. \end{aligned}$$

In equation (10), the $u_{i'l'}$ and u_{il} denote the radial part of the proton-neutron wave functions and the dependancy on the target deformation is included in the angular mometum coupling coefficients and in the expansion $v_p^{(\lambda)\sigma}$.

Convergence test: elastic and inel. cross sections for d+^{24}Mg and $E_d = 70.0$ MeV

Bin numbers for s and d waves:

0 bin: deuteron g.s.

1 bin to discretize the cont.

3 bins to discretize the cont.

4 bins to discretize the cont.

8 bins to discretize the cont.

10 bins to discretize the cont.

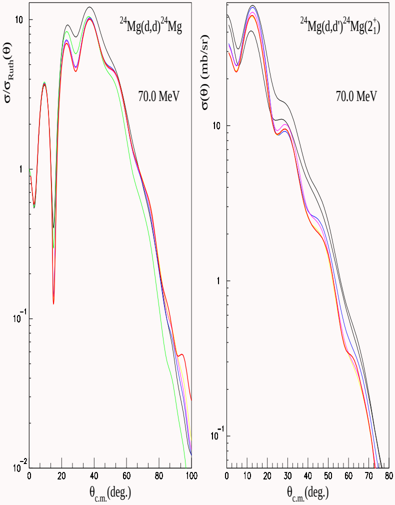

Elastic and inelastic cross sections (2_1^+ state) for a ^{24}Mg target and for $72.0 \leq E_d \leq 90.0$ MeV.

^{24}Mg(d,d)^{24}Mg at 90.0 MeV

^{24}Mg(d,d)^{24}Mg at 80.0 MeV

^{24}Mg(d,d)^{24}Mg at 78.0 MeV

^{24}Mg(d,d)^{24}Mg at 76.0 MeV

^{24}Mg(d,d)^{24}Mg at 74.0 MeV

^{24}Mg(d,d)^{24}Mg at 72.0 MeV

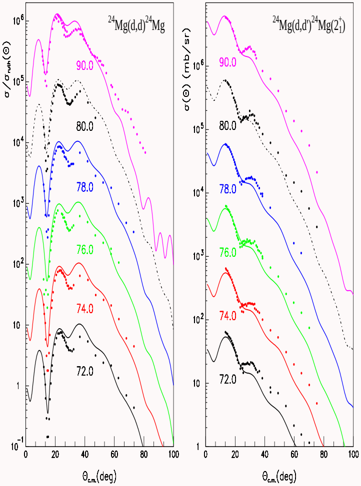

^{24}Mg(d,d')^{24}Mg*

^{24}Mg(d,d')^{24}Mg*

^{24}Mg(d,d')^{24}Mg*

^{24}Mg(d,d')^{24}Mg*

^{24}Mg(d,d')^{24}Mg*

^{24}Mg(d,d')^{24}Mg*

Vibrating target - The starting point: T. Tamura's work [4].

In [4], for a vibational target, the nucleon-nucleus coupling is given by:

$$V_{iA}(\vec{r}_i) = \sum_{t,\lambda} \hat{\lambda}(-1)^{\lambda+1} v_\lambda^{(t)}(r_i) \left[Q_\lambda^{(t)} \otimes Y_\lambda(\hat{r}_i) \right]_0^{(0)} .$$

$$r_i^\lambda Y_\mu^\lambda(\hat{r}_i) = \sum_{0\le p\le\lambda} \frac{\sqrt{4\pi(2\lambda+1)!} x_i^p R^p y_i^p \rho^{\lambda-p}}{\sqrt{(2p+1)!(2(\lambda-p)+1)!}} \left[Y^p(\hat{R}) \otimes Y^{\lambda-p}(\hat{\rho}) \right]_\mu^\lambda .$$

Thus

$$\begin{aligned} V_{iA}(\vec{r}_i) &= \sum_{t,\lambda} \hat{\lambda}(-1)^{\lambda+1} \frac{v_\lambda^{(t)}(r_i)}{r_i^\lambda} \sum_{0\le p\le\lambda} \frac{\sqrt{4\pi(2\lambda+1)!} x_i^p R^p y_i^p \rho^{\lambda-p}}{\sqrt{(2p+1)!(2(\lambda-p)+1)!}} \\ &\quad \left[Q_\lambda^{(t)} \otimes \left[Y^p(\hat{R}) \otimes Y^{\lambda-p}(\hat{\rho}) \right]^\lambda \right]_0^{(0)} \\ &= \sum_{t,\lambda,p,\mu} \hat{\lambda}(-1)^{\lambda+1} \frac{v_\lambda^{(t)}(r_i)}{r_i^\lambda} \langle \lambda\mu; \lambda-\mu|00\rangle \frac{\sqrt{4\pi(2\lambda+1)!} x_i^p R^p y_i^p \rho^{\lambda-p}}{\sqrt{(2p+1)!(2(\lambda-p)+1)!}} \\ &\quad Q_{\lambda\mu}^{(t)} \cdot \left[Y^p(\hat{R}) \otimes Y^{\lambda-p}(\hat{\rho}) \right]_\mu^\lambda . \end{aligned}$$

Vibrating target - Form factors.

For a vibrating nucleus, the following set of coupled differential equations satisfied by the radial parts $u_c^J(R)$ ($c = (i\,(lS)I_p\,L\,I_t\,J_T)$) of the wave functions have to be solved:

$$\left(-\frac{\hbar^2}{2\mu_R}\frac{d^2}{dR^2} + \frac{\hbar^2 L(L+1)}{2\mu_R R^2} + V_p^{(Coul)} - E_i\right) u_c^J(R) = -\sum_{c'} V_{cc'}^J(R) u_{c'}^J(R)\,,$$

where the form factors are given by

$$\begin{aligned}
V_{cc'}(R) \;=\; & \sum_{t\lambda p\sigma l'' L''} \frac{(-1)^{\tilde{R}_0}\sqrt{(2\lambda+1)!}}{4\pi\sqrt{(2p+1)!(2(\lambda-p)+1)!}} \widehat{L''}^2 \widehat{l''}^2 \hat{p}\widehat{(\lambda-p)} \\
& \hat{l}\hat{I}_p\hat{L}\hat{J}\widehat{l'}\hat{I}'_p\hat{L}'\hat{J}' \int u_l(\rho) u_{l''}(\rho) v_{\lambda p}^{\sigma(t)}(R,\rho) d\rho \\
& \begin{pmatrix} \sigma & p & L'' \\ 0 & 0 & 0 \end{pmatrix} \begin{pmatrix} \sigma & (\lambda-p) & l'' \\ 0 & 0 & 0 \end{pmatrix} \begin{pmatrix} l & l' & l'' \\ 0 & 0 & 0 \end{pmatrix} \\
& \begin{pmatrix} L & L' & L'' \\ 0 & 0 & 0 \end{pmatrix} \begin{Bmatrix} \lambda & l'' & L'' \\ \sigma & p & (\lambda-p) \end{Bmatrix} \begin{Bmatrix} J & I_t & J_T \\ I'_t & J' & \lambda \end{Bmatrix} \\
& \begin{Bmatrix} I_p & L & J \\ l'' & L'' & \lambda \\ I'_p & L' & J' \end{Bmatrix} \langle I'_t\, n'_{ph} \parallel Q^{(t)\lambda} \parallel n_{ph}\, I_t \rangle\, i^{L+l-(L'+l')} \delta_{ss'}\,.
\end{aligned}$$

Concluding remarks about this brief overview of the formalism.

We have built a framework to compute cross elastic, breakup and inelastic cross sections within a coupled channel formalism for spherical, rotational and vibrational targets by a folding the optical potential with the deuteron w.f. and the breakup states.

Excitation functions.

The cross section for a given process can be written as:

$$\sigma(E_d) = \sigma_{\text{Direct}}(E_d) + \sigma_{\text{Preq.}}(E_d) + \sigma_{\text{CN}}(E_d)$$

where E_d the deuteron incident energy.
For the (d,p) reaction, the aim of our approach is to include a direct component computed with the CDCC+DWBA approach.

$$\sigma^{(d,p)}_{\text{Direct}}(E_d) = \sum_{i \leq i_{\max}, l_n, j_n} \sigma_{l_n, j_n}(E_{x,i}, E_d)$$

where l_n and $j_n = l_n \pm 1/2$ denote the orbital angular momentum and spin of captured neutron, respectively while $E_{x,i}$ is the excitation energy of the occupied level. $i_{\max}$ depends on the incident energy and on the reaction Q-value.
Note that this idea is not new (e.g. it has been recently used by P. Bém *et al* [5]).

Excitation functions.

How to compute this direct component?

$$\sigma_{l_n,j_n}(E_{x,i}, E_d) = \int \frac{d\sigma_{l_n,j_n}}{d\Omega}(E_{x,i}, E_d)d\Omega = \int S_{l_n,j_n,i}\frac{d\sigma^{\text{calc.}}_{l_n,j_n}}{d\Omega}(E_{x,i}, E_d)d\Omega$$

Thus we need to

- compute the theoretical cross sections for the largest set of excited levels;
- compare the calculated differential cross sections with some experimental data;
- deduce the spectroscopic factor $S_{l_n,j_n,i}$ for each level;
- add all the contributions.

There are some drawbacks:

- how to build the largest set of excited levels?
- some spectroscopic factors $S_{l_n,j_n,i}$ are not known very accurately (they depend on the data used to extract them...);
- sometimes no data are available;
- computation is time consuming.

Excitation functions.

From some computation, it has been observed that the shape of excitation function does not strongly depend on $E_{x,i}$ but mainly on l_n. Thus we will replace

$$\sigma^{\text{calc.}}_{l_n,j_n}(E_{x,i}, E_d) \approx \tilde{\sigma}_{l_n,j_n}(E_d)$$

where $\tilde{\sigma}_{l_n,j_n}(E_d)$ is computed for a neutron state with an arbitrarly chosen excitation energy (ground state...) and with the same quantum numbers. Therefore

$$\begin{aligned}
\sigma^{(d,p)}_{\text{Direct}}(E_d) &= \sum_{i \le i_{\max}, l_n, j_n} \sigma_{l_n,j_n}(E_{x,i}, E_d) = \sum_{i \le i_{\max}, l_n, j_n} S_{l_n,j_n,i}\sigma^{\text{calc.}}_{l_n,j_n}(E_{x,i}, E_d) \\
&\approx \sum_{i \le i_{\max}, l_n, j_n} S_{l_n,j_n,i}\tilde{\sigma}_{l_n,j_n}(E_d) \approx \sum_{l_n,j_n} \sum_{i \le i_{\max}} S_{l_n,j_n,i}\tilde{\sigma}_{l_n,j_n}(E_d) .
\end{aligned}$$

Denoting $\sum_{i \le i_{\max}} S_{l_n,j_n,i} = W_{l_n,j_n}(E_d)$, we get that:

$$\sigma^{(d,p)}_{\text{Direct}}(E_d) \approx \sum_{l_n,j_n} W_{l_n,j_n}(E_d)\,\tilde{\sigma}_{l_n,j_n}(E_d) .$$

Excitation functions.

Thus we have obtained that

$$\sigma^{(d,p)}_{\text{Direct}}(E_d) \quad \approx \quad \sum_{l_n, j_n} W_{l_n, j_n}(E_d)\, \tilde{\sigma}_{l_n, j_n}(E_d)\,,$$

where the W_{l_n, j_n}'s are increasing functions of E_d.
Moreover, since it is expected that

$$\lim_{E_d \to \infty} W_{l_n, j_n}(E_d) = \omega_{l_n, j_n}\,,$$

for large incident energy, we should get

$$\sigma^{(d,p)}_{\text{Direct}}(E_d) \quad \underset{\infty}{\approx} \quad \sum_{l_n, j_n} \omega_{l_n, j_n}\, \tilde{\sigma}_{l_n, j_n}(E_d)\,.$$

CDCC*-DWBA

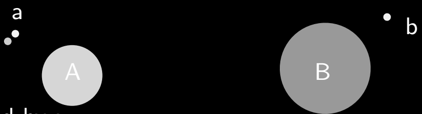

The system is described by :

$$\Psi_{\text{model}} = u_\alpha(\vec{r}_\alpha)\psi_\alpha(x_\alpha) + u_\beta(\vec{r}_\beta)\psi_\beta(x_\beta)$$

where α and β denote two partitions of the system : $\alpha = A + a$, $\beta = B + b$ and the $u_\alpha(\vec{r}_\alpha)$, $u_\beta(\vec{r}_\beta)$ are unknown functions.
For each partition, one can define a basis :

$$\Psi_\alpha = \delta_\alpha(\vec{r} - \vec{r}_\alpha)\psi_\alpha(x_\alpha) \text{ and } \Psi_\beta = \delta_\beta(\vec{r} - \vec{r}_\beta)\psi_\beta(x_\beta)\,.$$

The Schrödinger Equation reads :

$$\hat{H}\,\Psi_{\text{model}} = E\,\Psi_{\text{model}}\,.$$

Thus one can get :

$$\langle\Psi_\alpha|\left(\hat{H} - E\right)\Psi_{\text{model}}\rangle = 0 \;\text{ and }\; \langle\Psi_\beta|\left(\hat{H} - E\right)\Psi_{\text{model}}\rangle = 0\,.$$

CDCC*-DWBA.

$$\left\{\begin{array}{lcl} \left[E_\alpha - K_\alpha - \langle\alpha|V_{\alpha\alpha}|\alpha\rangle\right] u_\alpha(\vec{r}_\alpha) & = & \int d\vec{r}_\beta d\chi_\alpha \psi_\alpha^* V_{\alpha\beta}(\vec{r}_\alpha,\vec{r}_\beta)\psi_\beta u_\beta(\vec{r}_\beta) \\ \left[E_\beta - K_\beta - \langle\beta|V_{\beta\beta}|\beta\rangle\right] u_\beta(\vec{r}_\beta) & = & \int d\vec{r}_\alpha d\chi_\beta \psi_\beta^* V_{\beta\alpha}(\vec{r}_\alpha,\vec{r}_\beta)\psi_\alpha u_\alpha(\vec{r}_\alpha) \end{array}\right.$$

Assuming that the coupling in the first equation can be neglected then the following equations are obtained :

$$\left\{\begin{array}{lcl} \left[E_\alpha - K_\alpha - \langle\alpha|V_{\alpha\alpha}|\alpha\rangle\right] u_\alpha(\vec{r}_\alpha) & \approx & 0 \\ \left[E_\beta - K_\beta - \langle\beta|V_{\beta\beta}|\beta\rangle\right] u_\beta(\vec{r}_\beta) & = & \int d\vec{r}_\alpha d\chi_\beta \psi_\beta^* V_{\beta\alpha}(\vec{r}_\alpha,\vec{r}_\beta)\psi_\alpha u_\alpha(\vec{r}_\alpha) \end{array}\right.$$

Thus

- for the channel α, one gets an equation which describes an elastic scattering (it will be derived from a CDCC* calculation) ;
- for the channel β, one gets a differential equation with a source term derived from optical potentials $V_{\alpha\beta}$ and from the elastic wave function u_α.

The cross sections are derived from u_α and u_β.

Cross sections for $Z = 26$ and $N = 32$: ^{58}Fe(d,p)^{59}Fe - neutron w.f. and $d\sigma/d\Omega$.

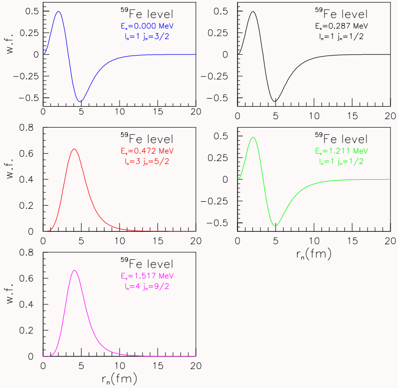

Figure: Five levels in ^{59}Fe.

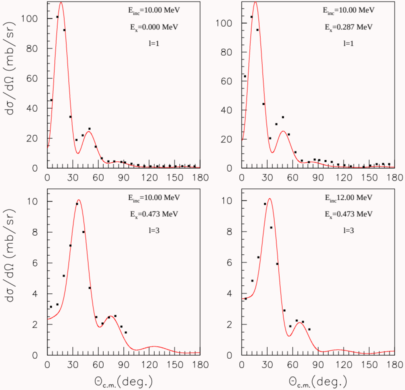

Figure: ^{58}Fe(d,p)^{59}Fe: $d\sigma/d\Omega$.

Cross sections for $Z = 26$ and $N = 32$: ^{58}Fe(d,p)^{59}Fe - $d\sigma/d\Omega$.

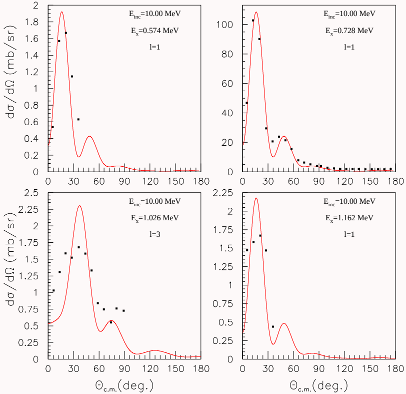

Figure: ^{58}Fe(d,p)^{59}Fe: $d\sigma/d\Omega$.

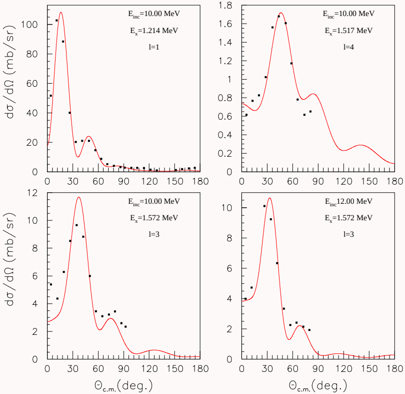

Figure: ^{58}Fe(d,p)^{59}Fe: $d\sigma/d\Omega$.

Cross sections for $Z = 26$ and $N = 32$: ^{58}Fe(d,p)^{59}Fe - $d\sigma/d\Omega$.

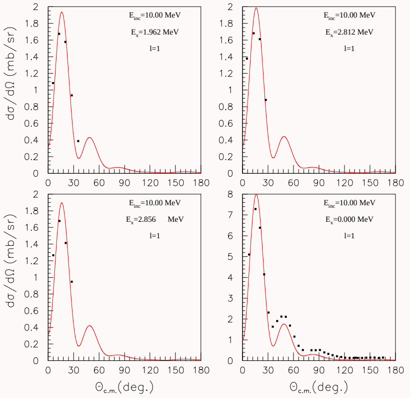

Figure: ^{58}Fe(d,p)^{59}Fe: $d\sigma/d\Omega$.

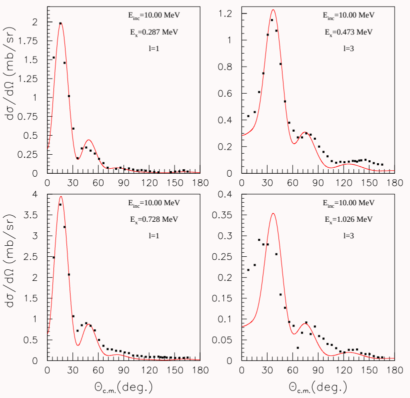

Figure: ^{58}Fe(d,p)^{59}Fe: $d\sigma/d\Omega$.

Cross sections for $Z = 28$ and $N = 32$: ^{58}Fe(d,p)^{59}Fe - Excitation function.

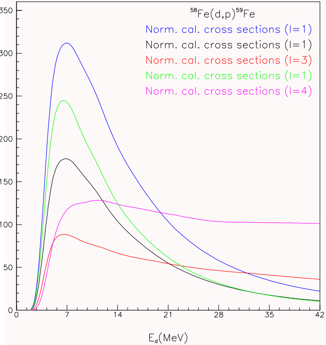

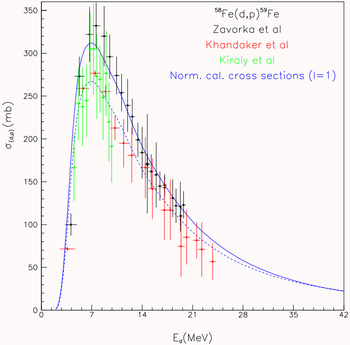

$\sigma^{\text{calc.}}_{l_n,j_n}(E_{x,i}, E_d)$ for five levels with

- $E_x = 0.000$ MeV, $l_n = 1$ and $j_n^\pi = 3/2^-$
- $E_x = 0.287$ MeV, $l_n = 1$ and $j_n^\pi = 1/2^-$
- $E_x = 0.472$ MeV, $l_n = 3$ and $j_n^\pi = 5/2^-$
- $E_x = 1.211$ MeV, $l_n = 1$ and $j_n^\pi = 1/2^-$
- $E_x = 1.517$ MeV, $l_n = 4$ and $j_n^\pi = 9/2^+$.

Comparison between the measured cross sections and

$$\sum_{l_n,j_n} \omega_{l_n,j_n} \tilde{\sigma}_{l_n,j_n}(E_d).$$

Cross sections for $Z = 13$ and $N = 14$: ^{27}Al(d,p)^{28}Al - Excitation function.

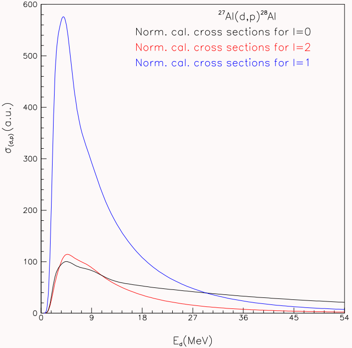

Figure: ^{27}Al(d,p)^{28}Al.

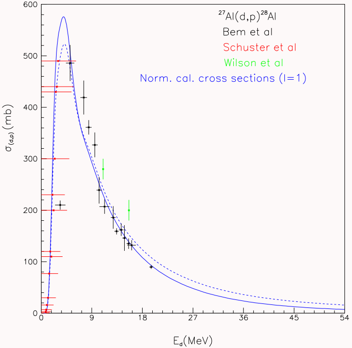

Figure: ^{27}Al(d,p)^{28}Al.

$\sigma^{\text{calc.}}_{l_n,j_n}(E_{x,i}, E_d)$ for 3 levels with

- $E_x = 0.000$ MeV, $l_n = 0$ and $j_n^\pi = 1/2^+$
- $E_x = 0.287$ MeV, $l_n = 2$ and $j_n^\pi = 3/2^+$
- $E_x = 0.472$ MeV, $l_n = 1$ and $j_n^\pi = 3/2^-$.

Comparison between the measured cross sections and

$$\sum_{l_n,j_n} \omega_{l_n,j_n}\, \tilde{\sigma}_{l_n,j_n}(E_d).$$

Cross sections for $Z = 27$ and $N = 32$: ^{59}Co(d,p)^{60}Co - $d\sigma/d\Omega$.

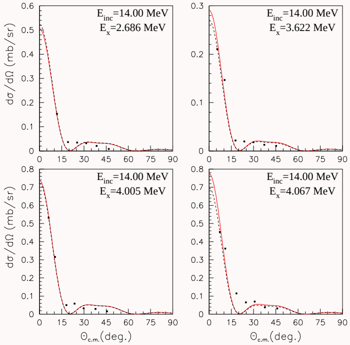

Figure: ^{59}Co(d,p)^{60}Co for $l_n = 0$.

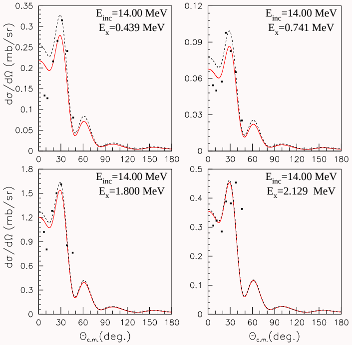

Figure: ^{59}Co(d,p)^{60}Co for $l_n = 3$.

Cross sections for $Z = 27$ and $N = 32$: ^{59}Co(d,p)^{60}Co - $d\sigma/d\Omega$ - Excitation function.

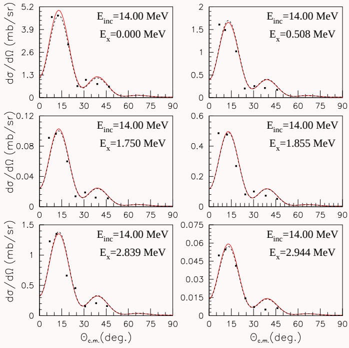

Figure: ^{59}Co(d,p)^{60}Co for $l_n = 1$.

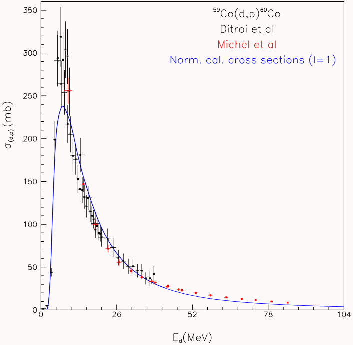

Figure: ^{59}Co(d,p)^{60}Co.

Cross sections for $Z = 33$ and $N = 42$: ^{75}As(d,p)^{76}As - $d\sigma/d\Omega$.

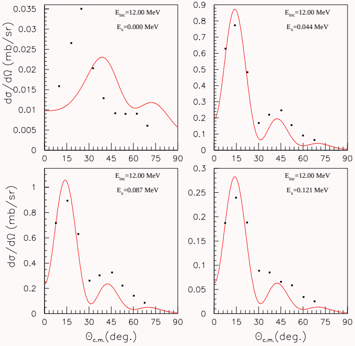

Figure: ^{75}As(d,p)^{76}As.

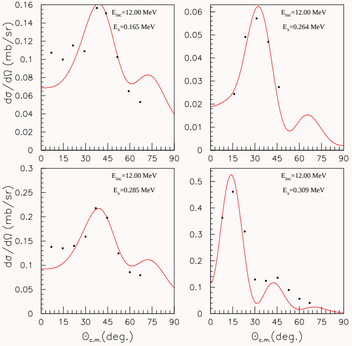

Figure: ^{75}As(d,p)^{76}As.

Cross sections for $Z = 33$ and $N = 42$: ^{75}As(d,p)^{76}As - $d\sigma/d\Omega$.

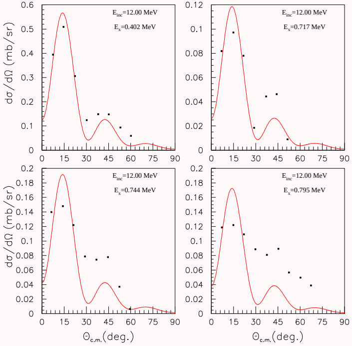

Figure: ^{75}As(d,p)^{76}As.

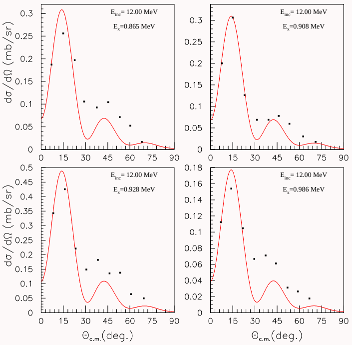

Figure: ^{75}As(d,p)^{76}As.

Cross sections for $Z = 33$ and $N = 42$: ^{75}As(d,p)^{76}As - Excitation function.

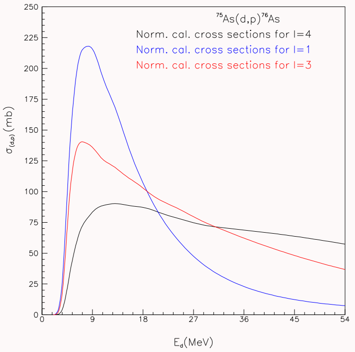

Figure: ^{75}As(d,p)^{76}As.

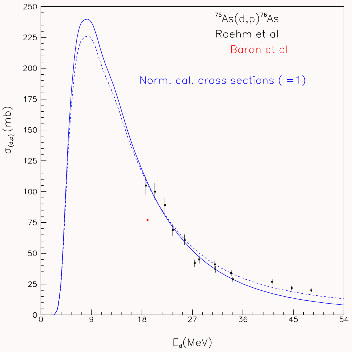

Figure: ^{75}As(d,p)^{76}As.

$\sigma^{\text{calc.}}_{l_n,j_n}(E_{x,i}, E_d)$ for 3 levels with

- $E_x = 0.000$ MeV, $l_n = 4$ and $j_n^\pi = 7/2^+$
- $E_x = 0.287$ MeV, $l_n = 1$ and $j_n^\pi = 3/2^-$
- $E_x = 0.472$ MeV, $l_n = 3$ and $j_n^\pi = 5/2^-$.

Comparison between the measured cross sections and

$$\sum_{l_n,j_n} \omega_{l_n,j_n}\, \tilde{\sigma}_{l_n,j_n}(E_d).$$

Cross sections for $Z = 35$ and $N = 46$: ^{81}Br(d,p)^{82}Br - $d\sigma/d\Omega$.

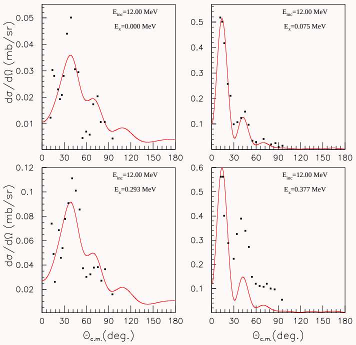

Figure: ^{81}Br(d,p)^{82}Br.

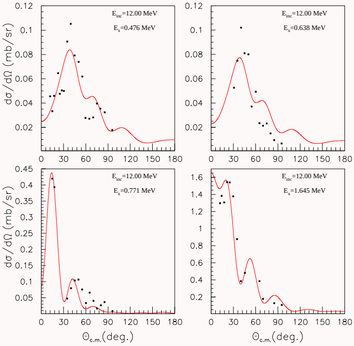

Figure: ^{81}Br(d,p)^{82}Br.

Cross sections for $Z = 35$ and $N = 46$: ^{81}Br(d,p)^{82}Br - Excitation function.

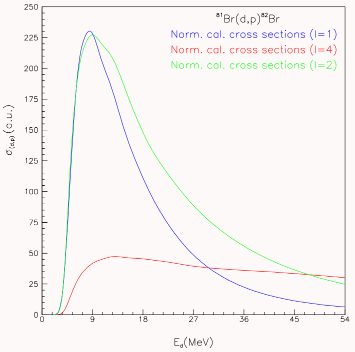

Figure: ^{81}Br(d,p)^{82}Br.

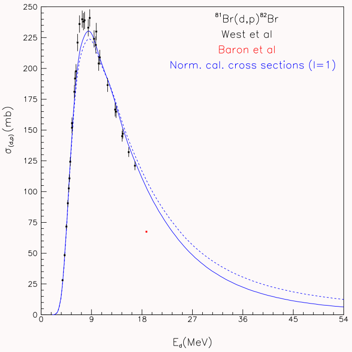

Figure: ^{81}Br(d,p)^{82}Br.

$\sigma^{\text{calc.}}_{l_n,j_n}(E_{x,i}, E_d)$ for 3 levels with

- $E_x = 0.000$ MeV, $l_n = 2$ and $j_n^\pi = 9/2^+$
- $E_x = 0.075$ MeV, $l_n = 1$ and $j_n^\pi = 1/2^-$
- $E_x = 1.650$ MeV, $l_n = 2$ and $j_n^\pi = 3/2^+$.

Comparison between the measured cross sections and

$$\sum_{l_n,j_n} \omega_{l_n,j_n} \tilde{\sigma}_{l_n,j_n}(E_d).$$

Cross sections for $Z = 36$ and $N = 48$: ^{84}Kr(d,p)^{85}Kr - $d\sigma/d\Omega$.

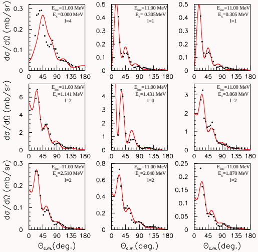

Figure: ^{84}Kr(d,p)^{85}Kr.

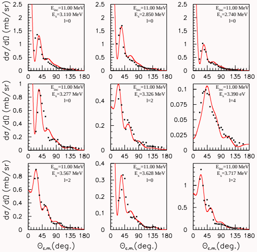

Figure: ^{84}Kr(d,p)^{85}Kr.

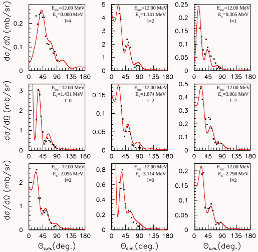

Figure: ^{84}Kr(d,p)^{85}Kr.

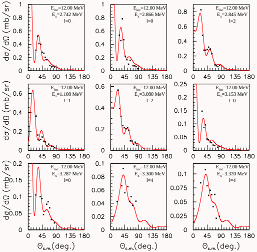

Figure: ^{84}Kr(d,p)^{85}Kr.

Cross sections for $Z = 36$ and $N = 48, 50$: ^{86}Kr(d,p)^{87}Kr and ^{84}Kr(d,p)^{85m}Kr.

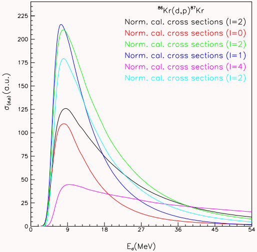

Figure: ^{86}Kr(d,p)^{87}Kr.

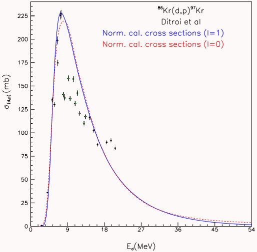

Figure: ^{86}Kr(d,p)^{87}Kr.

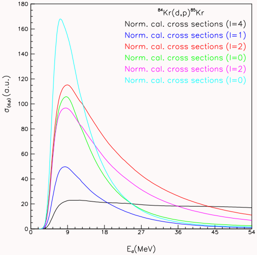

Figure: ^{84}Kr(d,p)^{85}Kr.

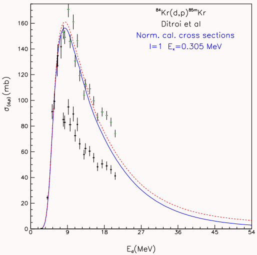

Figure: ^{84}Kr(d,p)^{85m}Kr.

Cross sections for $Z = 46$ and $N = 62$: ^{108}Pd(d,p)^{109}Pd - Excitation function.

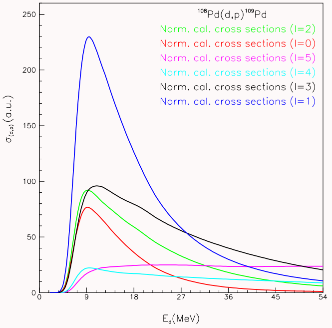

Figure: ^{108}Pd(d,p)^{109}Pd.

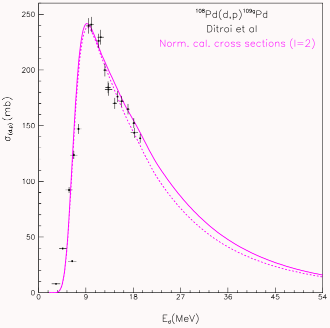

Figure: ^{108}Pd(d,p)^{109}Pd.

$\sigma^{\text{calc.}}_{l_n,j_n}(E_{x,i}, E_d)$ for 6 levels with

- $E_x = 0.000$ MeV, $l_n = 2$ and $j_n^\pi = 5/2^+$
- $E_x = 0.113$ MeV, $l_n = 0$ and $j_n^\pi = 1/2^+$
- $E_x = 0.188$ MeV, $l_n = 5$ and $j_n^\pi = 11/2^-$
- $E_x = 0.245$ MeV, $l_n = 4$ and $j_n^\pi = 7/2^+$
- $E_x = 0.339$ MeV, $l_n = 3$ and $j_n^\pi = 5/2^-$

Comparison between the measured cross sections and

$$\sum_{l_n,j_n} \omega_{l_n,j_n}\, \tilde{\sigma}_{l_n,j_n}(E_d).$$

Cross sections for $Z = 46$ and $N = 64$: ^{110}Pd(d,p)^{111m}Pd - Excitation function.

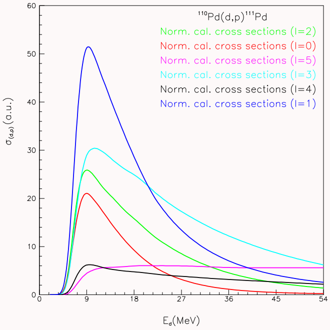

Figure: ^{110}Pd(d,p)^{111}Pd.

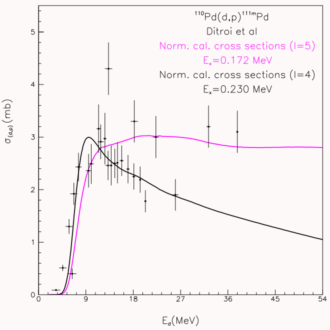

Figure: ^{110}Pd(d,p)^{111m}Pd.

$\sigma^{\text{calc.}}_{l_n,j_n}(E_{x,i}, E_d)$ for 6 levels with

- $E_x = 0.000$ MeV, l_n=2 and $j_n^\pi = 5/2^+$
- $E_x = 0.072$ MeV, l_n=0 and $j_n^\pi = 1/2^+$
- $E_x = 0.172$ MeV, l_n=5 and $j_n^\pi = 11/2^-$
- $E_x = 0.191$ MeV, l_n=3 and $j_n^\pi = 7/2^-$
- $E_x = 0.230$ MeV, l_n=4 and $j_n^\pi = 7/2^+$

Comparison between the measured cross sections and

$$\sum_{l_n,j_n} \omega_{l_n,j_n}\, \tilde{\sigma}_{l_n,j_n}(E_d).$$

Cross sections for $Z = 47$ and $N = 62$: ^{109}Ag(d,p)^{110}Ag - $d\sigma/d\Omega$.

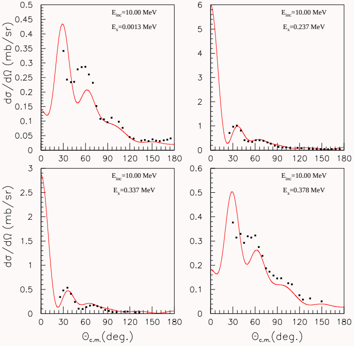

Figure: ^{109}Ag(d,p)^{110}Ag.

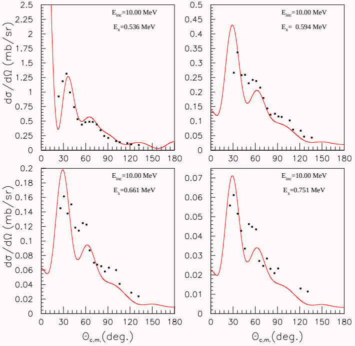

Figure: ^{109}Ag(d,p)^{110}Ag.

Cross sections for $Z = 47$ and $N = 62$: ^{109}Ag(d,p)^{110}Ag - Excitation function.

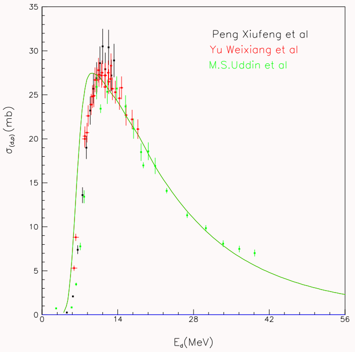

Figure: ^{109}Ag(d,p)^{110}Ag.

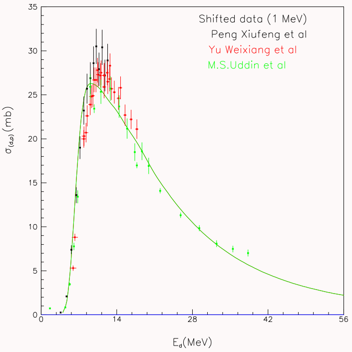

Figure: ^{109}Ag(d,p)^{110}Ag.

$\sigma^{\text{calc.}}_{l_n,j_n}(E_{x,i}, E_d)$ for 3 levels with

- $E_x = 0.013$ MeV, l_n=2 and $j_n^\pi = 3/2^+$
- $E_x = 0.237$ MeV, l_n=0 and $j_n^\pi = 1/2^+$
- $E_x = 0.378$ MeV, l_n=2 and $j_n^\pi = 3/2^+$.

Comparison between the measured cross sections and

$$\sum_{l_n,j_n} \omega_{l_n,j_n} \tilde{\sigma}_{l_n,j_n}(E_d).$$

Cross sections for $Z = 58$ and $N = 82$: ^{140}Ce(d,p)^{141}Ce - Excitation function.

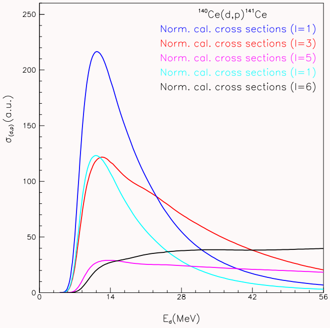

Figure: ^{140}Ce(d,p)^{141}Ce.

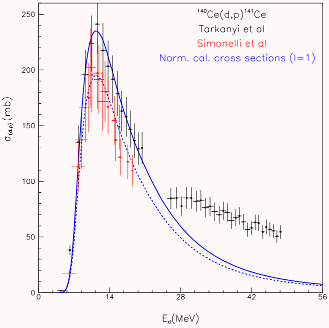

Figure: ^{140}Ce(d,p)^{141}Ce.

$\sigma^{\text{calc.}}_{l_n,j_n}(E_{x,i}, E_d)$ for 5 levels with

- $E_x = 0.000$ MeV, l_n=3 and $j_n^\pi = 7/2^-$
- $E_x = 0.662$ MeV, l_n=1 and $j_n^\pi = 3/2^-$
- $E_x = 1.337$ MeV, l_n=1 and $j_n^\pi = 1/2^-$
- $E_x = 1.354$ MeV, l_n=5 and $j_n^\pi = 9/2^-$
- $E_x = 1.368$ MeV, l_n=6 and $j_n^\pi = 13/2^+$.

Comparison between the measured cross sections and

$$\sum_{l_n,j_n} \omega_{l_n,j_n}\, \tilde{\sigma}_{l_n,j_n}(E_d).$$

Cross sections for $Z = 58$ and $N = 84$: ^{142}Ce(d,p)^{143}Ce - Excitation function.

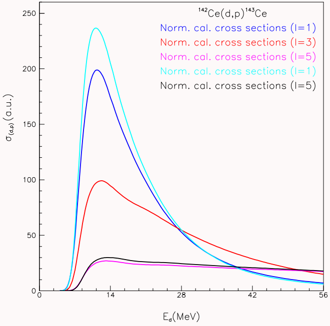

Figure: ^{142}Ce(d,p)^{143}Ce.

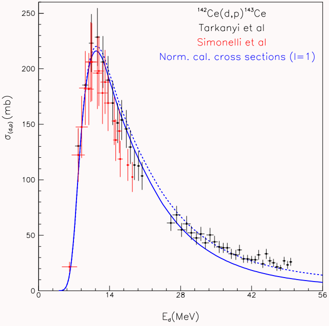

Figure: ^{142}Ce(d,p)^{143}Ce.

$\sigma^{\text{calc.}}_{l_n,j_n}(E_{x,i}, E_d)$ for 5 levels with

- $E_x = 0.000$ MeV, l_n=1 and $j_n^\pi = 3/2^-$
- $E_x = 0.019$ MeV, l_n=3 and $j_n^\pi = 5/2^-$
- $E_x = 0.662$ MeV, l_n=5 and $j_n^\pi = 9/2^-$
- $E_x = 0.808$ MeV, l_n=1 and $j_n^\pi = 3/2^-$
- $E_x = 1.222$ MeV, l_n=5 and $j_n^\pi = 9/2^-$.

Comparison between the measured cross sections and

$$\sum_{l_n,j_n} \omega_{l_n,j_n}\, \tilde{\sigma}_{l_n,j_n}(E_d).$$

Cross sections for $Z = 59$ and $N = 82$: ^{141}Pr(d,p)^{142}Pr - Excitation function.

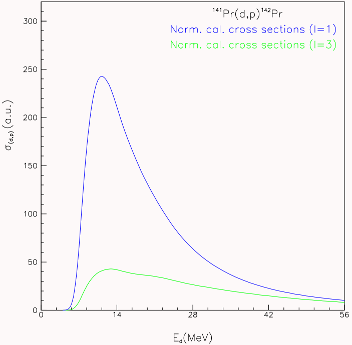

Figure: ^{141}Pr(d,p)^{142}Pr.

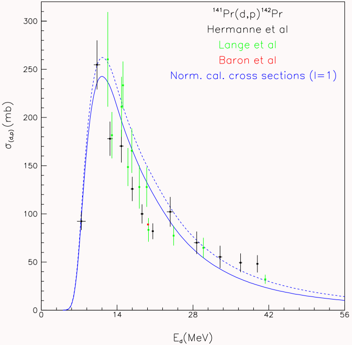

Figure: ^{141}Pr(d,p)^{142}Pr.

$\sigma^{\text{calc.}}_{l_n,j_n}(E_{x,i}, E_d)$ for 3 levels with

- $E_x = 0.000$ MeV, l_n=3 and $j_n^\pi = 5/2^-$
- $E_x = 0.637$ MeV, l_n=1 and $j_n^\pi = 3/2^-$

Comparison between the measured cross sections and

$$\sum_{l_n,j_n} \omega_{l_n,j_n}\, \tilde{\sigma}_{l_n,j_n}(E_d).$$

Cross sections for $Z = 67$ and $N = 98$: ^{165}Ho(d,p)^{166}Ho - Excitation function.

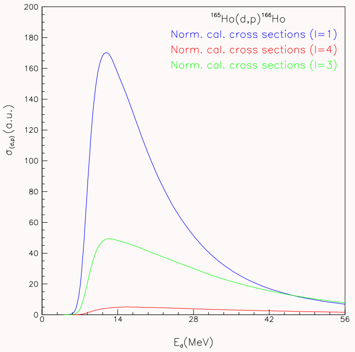

Figure: ^{165}Ho(d,p)^{166}Ho.

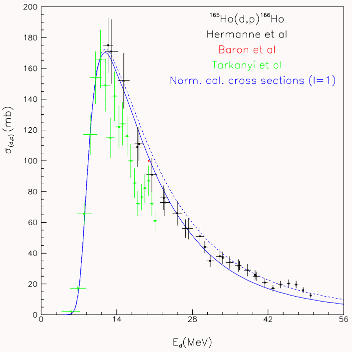

Figure: ^{165}Ho(d,p)^{166}Ho.

$\sigma^{\text{calc.}}_{l_n,j_n}(E_{x,i}, E_d)$ for 3 levels with

- $E_x = 0.000$ MeV, l_n=4 and $j_n^\pi = 7/2^+$
- $E_x = 0.190$ MeV, l_n=1 and $j_n^\pi = 3/2^-$
- $E_x = 0.295$ MeV, l_n=3 and $j_n^\pi = 5/2^-$.

Comparison between the measured cross sections and

$$\sum_{l_n,j_n} \omega_{l_n,j_n}\, \tilde{\sigma}_{l_n,j_n}(E_d).$$

Cross sections for $Z = 72$ and $N = 108$: ^{180}Hf(d,p)^{181}Hf - Excitation function.

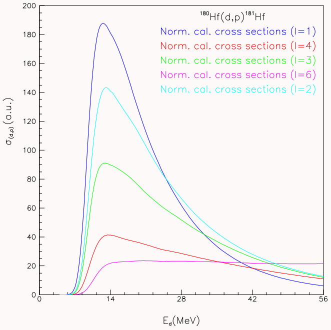

Figure: ^{180}Hf(d,p)^{181}Hf.

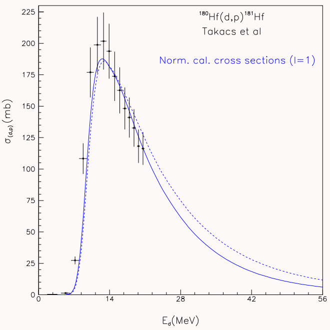

Figure: ^{180}Hf(d,p)^{181}Hf.

$\sigma^{\text{calc.}}_{l_n,j_n}(E_{x,i}, E_d)$ for 5 levels with

- $E_x = 0.000$ MeV, l_n=1 and $j_n^\pi = 1/2^-$
- $E_x = 0.068$ MeV, l_n=4 and $j_n^\pi = 9/2^+$
- $E_x = 0.099$ MeV, l_n=3 and $j_n^\pi = 5/2^-$
- $E_x = 0.471$ MeV, l_n=6 and $j_n^\pi = 11/2^+$
- $E_x = 0.902$ MeV, l_n=2 and $j_n^\pi = 5/2^+$.

Comparison between the measured cross sections and

$$\sum_{l_n,j_n} \omega_{l_n,j_n}\, \tilde{\sigma}_{l_n,j_n}(E_d).$$

Summary.

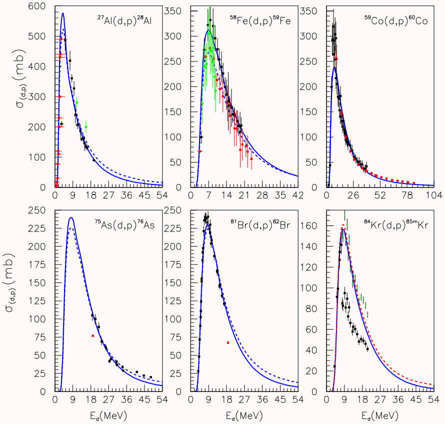

Figure: Excitation functions for (d,p) reaction.

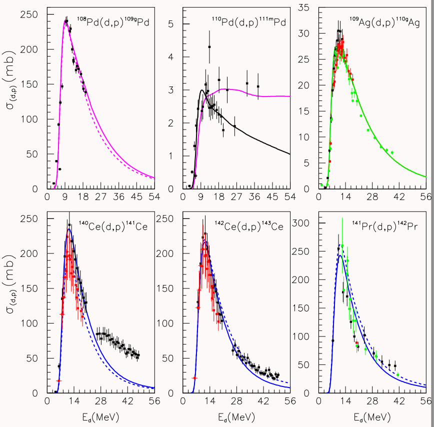

Figure: Excitation functions for (d,p) reaction.

Trend of $\omega_{l_n=1}$.

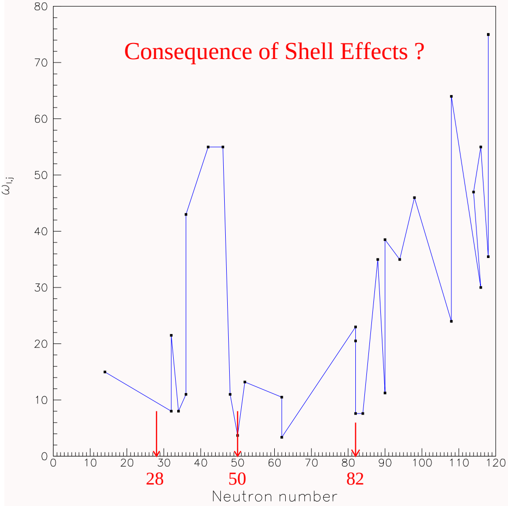

Figure: ω_{l_n,j_n} as function of the neutron number.

$\omega_{l_n=1}$ as function of the neutron number:

- It seems that there are some shell effects.
- What happens for $N \geq 120$?

Conclusion - Summary & Outlook.

Within this talk, I have tried to present

1. the main ideas of the CDCC approach,
2. some extensions including the target excitations,
3. some applications:
    1. The CDCC* can be used to compute elastic and inelastic cross sections.
    2. For transfer reactions, the differential cross sections agree well with the experimental data.
    3. We have proposed a phenomenological approach based on the CDCC calculations to get the (d,p) excitation functions. The calculations have been presented for 29 nuclei and for incident energies ranging from 2 MeV to more than 50 MeV.
       Amazingly, a quite good agreement has been found between the calculated cross sections and the measured ones.
       Similar computations have been performed for 132 nuclei : some experimental data are needed to compare with these results.

Conclusion - Summary & Outlook.

Many questions remain to be answered:

1. Its seems that only the $l_n = 1$ or $l_n = 0$ components contribute to the cross sections (d,p). Why? Is it due to the centrifugal barrier?
2. What does it tell us about the reaction mechanism for the (d,p) process? Is it mainly a direct reaction?
3. Can we predict the ω's from a "microscopic" approach?
4. Some preliminary calculations have been performed for (d,n) cross sections : some discrepancies have been observed with the measured excitation functions. Under investigation...

Moreover, can we conclude that "prédire n'est pas expliquer" (René Thom)?

Acknowledgment.

- First of all, I thank the organizers for giving me this opportunity to present these results.
- I thank my colleagues at Bruyères-le-Chatel.
- I also thank Nick Keeley and Valérie Lapoux.

Thank you for your attention.

Acknowledgment.

- First of all, I thank the organizers for giving me this opportunity to present these results.
- I thank my colleagues at Bruyères-le-Chatel.
- I also thank Nick Keeley and Valérie Lapoux.

Thank you for your attention.

- N. Soppera, E. Dupont, M. Bossant, JANIS Book of deuteron-induced cross-sections Comparison of evaluated and experimental data from ENDF/B-VII.1, TENDL-2011 and EXFOR.
- N. Austern, Y. Iseri, M. Kamimura, M. Kawai, G.H. Rawitscher and M. Yahiro, Phys. Rep. 154 (1987) 125.
- M. Yahiro, Y. Iseri, H. Kameyama, M. Kamimura and M. Kawai, Prog. Theor. Phys. Suppl. 89 (1986) 32.
- T. Tamura, Rev. Mod. Phys. **37** (1965) 679.
- P. Bém *et al*, Phys. Rev. C **79** (2009) 044610; E. Šimečková *et al*, Phys. Rev. C **84** (2011) 014605; M. Avrigeanu *et al*, Phys. Rev. C **88** (2013) 014612; M. Avrigeanu *et al*, Phys. Rev. C **89** (2014) 044613.